# Solving Few-Body Scattering Problems in a Discrete Representation by Using GPU

**O. A. Rubtsova, V. N. Pomerantsev and V. I. Kukulin**

*Skobeltsyn Institute of Nuclear Physics, Lomonosov Moscow State University, Moscow 119991, Russia*

**Abstract**

Different aspects of the Wave-Packet Continuum Discretization method are discussed in applications to few-body scattering problems. Scattering observables in multichannel two-body problems can be found by diagonalization of the total Hamiltonian in the free wave-packet basis without solving the scattering equations at all. In few-body case, wave functions and operators are projected into the discrete wave-packet representation which results in a matrix reduction of integral equations of the scattering theory. The necessary boundary conditions are taken into account by an employment of the finite-dimensional (matrix) representations for the free and channel resolvents. As a numerical illustration, we consider the *nd* scattering problem with realistic $NN$ interaction, which is solved via the highly parallelized computational scheme on an ordinary PC within the GPU technique.

**Keywords:** *Scattering theory; discretization of continuum; graphics processing unit*

## 1 Introduction

A consistent solution for few-body scattering problems has been done, as is well known, many years ago by Faddeev and Yakubovsky [1] which gave rise to an extensive few-body activity worldwide both in theory and experiment. However, a practical solving of such problems still presents a difficult numerical task in spite of a great progress in computational facilities. Alternatively, the methods which use $L_2$-normalized wave functions for continuum states in solving multi-channel and few-body scattering problems have been developed. Such methods are very useful nowadays in nuclear and atomic physics [2–5]. Some of them are adapted for treating the realistic interactions in few-nucleon systems (see the recent review [6]).

About a decade ago, our group in Moscow State University has developed an original approach [7–10] which allows to formulate problems in the continuum in terms of normalized analogs of initial scattering states, i. e., stationary wave packets (WPs) or eigendifferentials as they were introduced by Herman Weyl [11]. One of the central points of the approach is an analytical finite-dimensional representation for

*Proceedings of the International Conference 'Nuclear Theory in the Supercomputing Era — 2016' (NTSE-2016), Khabarovsk, Russia, September 19–23, 2016. Eds. A. M. Shirokov and A. I. Mazur. Pacific National University, Khabarovsk, Russia, 2018, p. 205.*

*http://www.ntse-2016.khb.ru/Proc/Rubtsova.pdf.*

the few-body free and channel resolvents. The solution scheme is realized in a discrete (on energy and momentum) representation allowing to replace few-body scattering integral equations by their matrix analogs. A detailed description of the entire wave-packet continuum discretization (WPCD) approach and its various applications can be found in our review paper [7].

The above WPCD method as well as a treatment of $L_2$ functions in the discretized continuum, have several important features [7]. First, according to the finite norms of states, one can take into account the long-range Coulomb interaction without any screening by using the Coulomb wave-packet formalism. Moreover, these normalized Coulomb WPs can be approximated in some appropriate $L_2$ basis and even in the basis of free WPs (the normalized analogs of the plane waves). Second, due to the matrix form of the resulting equations, there are no additional difficulties in treating non-local potentials (as well as complex-valued interaction operators). The numerical scheme remains the same. This fact is very important for the present direct nuclear reaction studies, where non-local interactions are employed instead of usual local energy-dependent potentials [12]. Another important feature is related to the fact that we use the integral equation formalism in the scattering theory with accurate approximations for the resolvents in the kernels which allows to avoid an explicit account of the boundary conditions. In particular, there are no difficulties to treat accurately closed channels in the coupled-channel problems [7].

In the present paper, we discuss mainly two issues of the general WPCD approach. A special attention is focused on the diagonalization technique, i. e., the discrete spectral shift (DSS) formalism, which allows to find scattering observables in a multichannel two-body problem by making use of spectral properties of the total and free Hamiltonians without solving scattering equations at all. The DSS method has a close relation to the Lüscher finite volume approach [13] which is well known in the lattice QCD applications [14]. Also our method has similar features with the SS-HORSE method which has been developed very recently [15, 16].

Another important theme studied here is a development of an efficient numerical scheme for a solution of few-body scattering problems in the Faddeev framework within the WPCD approach. Recently [9] we have performed a parallel optimization of our computational scheme for the *nd* elastic scattering problem and adapted it for a practical realization on a desk PC with the graphics processing unit (GPU). So, we describe the details of such an optimization in the present paper.

The paper is organized as follows. The definition of the stationary wave packets and their basic properties are given in Section 2. Section 3 is dedicated to the diagonalization technique which allows to find scattering observables as well as off-shell $t$ matrix in a multichannel scattering problem without solving the scattering theory equations. A brief description of the closed WPCD formalism in solving few-body scattering problems via the matrix analogs of scattering equations is given in Section 4. The details of a practical solution of the discretized Faddeev equation for the three-nucleon system by using the GPU, are presented in Section 5. We summarize the main results in the last Section 6.

# 2 Stationary wave packets and their properties

## 2.1 Stationary wave packets

Let us consider some two-body Hamiltonian $h = h_0 + v$ where $h_0$ is a free Hamiltonian (kinetic energy operator) and $v$ is an interaction potential, and divide the continuous spectrum of $h$ into a set of non-overlapping intervals $\{[\mathcal{E}_{k-1}, \mathcal{E}_k]\}_{k=1}^{N}$. The stationary WPs are constructed as integrals of exact scattering wave functions $|\psi_p\rangle$ over corresponding momentum intervals $\mathfrak{D}_k \equiv [p_{k-1}, p_k]$ (with $p_k = \sqrt{2m\mathcal{E}_k}$):

$$|z_k\rangle = \frac{1}{\sqrt{B_k}} \int_{\mathfrak{D}_k} f(p)\, |\psi_p\rangle\, dp, \quad B_k \equiv \int_{\mathfrak{D}_k} |f(p)|^2 dp, \tag{1}$$

where $m$ is the reduced mass of the system, $B_k$ and $f(p)$ are normalization factors and weight functions respectively which are interrelated.

The states (1) are well known as the Weyl's eigendifferentials [11]. The integration over the energy (or momentum) intervals is just enough to make normalized wave-functions for the continuum. Then a complete system of eigenfunctions of the Hamiltonian $h$, according to Weyl, can be constructed from its bound states $\{|\psi_n\rangle\}_{n=1}^{N_b}$ and eigendifferentials (see the details in Ref. [7]). In such a representation, the Hamiltonian $h$ as well as its resolvent $g(E) = [E + \mathrm{i}0 - h]^{-1}$ have explicit diagonal forms (see below).

These properties are valid not only for short-range potentials. In fact, one can build similar wave packets for a Hamiltonian which includes the long-range repulsive[1] Coulomb interaction, i. e.,

$$h_C = h_0 + \frac{z_1 z_2 e^2}{r}, \tag{2}$$

where $z_1$ and $z_2$ are the particle charges, $r$ is the distance between them. For this Hamiltonian, one can introduce the *Coulomb wave packets* $|x_k^C\rangle$ as the basis functions. These Coulomb WPs are built from the regular Coulomb wave functions $F_l(p, r)$ (for each partial wave $l$) by an integration over discretization intervals quite similarly to the general case [7]:

$$|x_k^C\rangle = \frac{1}{\sqrt{B_k}} \int_{\mathfrak{D}_k} \mathrm{d}p\, f(p)\, |F_l(p)\rangle. \tag{3}$$

The states (3) are normalized, so that they can be practically constructed using pseudostates of the Coulomb Hamiltonian (2) on some $L_2$ basis.

## 2.2 Discrete representation for the total resolvent

The most useful property of the WP states of some Hamiltonian $h$ is that one can construct a finite-dimensional representation for its resolvent $g(E) = [E + \mathrm{i}0 - h]^{-1}$. For this purpose, the projector onto the WP space $\mathfrak{p}$ should be defined:

$$\mathfrak{p} = \sum_{n=1}^{N_b} |\psi_n\rangle\langle\psi_n| + \sum_{k=1}^{N} |z_k\rangle\langle z_k|, \tag{4}$$

[1]The Coulomb attraction can be also treated in the WP approach, however it requires a separate study.

where $|\psi_n\rangle$ are the bound-state wave functions. So that, one gets analytically the finite-dimensional representation for the projected resolvent [7],

$$\mathfrak{g}(E) = \mathfrak{p}g(E)\mathfrak{p} = \sum_{n=1}^{N_b} \frac{|\psi_n\rangle\langle\psi_n|}{E - E_n} + \sum_{k=1}^{N} |z_k\rangle g_k(E)\langle z_k|, \tag{5}$$

where $E_n$ are bound-state energies, and the eigenvalues $g_k(E)$ do not depend on interaction but depend on discretization parameters only. The free and a repulsive Coulomb Hamiltonians have the same representations (without the bound-state contribution) in the free and Coulomb WP bases respectively.

## 2.3 Free wave-packets as a basis

The most useful examples of WP states are free WPs corresponding to the kinetic energy operator $h_0$ since they have explicit forms.

Indeed, in the momentum representation, the free WP functions are simple step-like functions [7]: they do not vanish only on the given discretization interval, i. e., only in the on-shell region. In this area they are completely determined by the weight function $f(p)$:

$$x_k(p) = \frac{f(p)\,\theta(p \in \mathfrak{D}_k)}{\sqrt{B_k}}, \tag{6}$$

where $\theta$ is the Heaviside step-like function which is equal to unity if $p \in \mathfrak{D}_k$ while outside it is equal to zero [7]. When $f(p) = 1$ (and $B_k = d_k$ where $d_k = p_k - p_{k-1}$ is the width of the corresponding momentum interval) all the wave functions in the momentum WP representation take a histogram form. Being generalized onto a few-body case, the free few-body WP basis functions are built as a direct products of step-like functions for each independent momentum variable. Thus, the whole few-body momentum space is replaced by a finite momentum lattice. In this sense, we refer to the free WP basis as *the lattice basis*.

From the practical point of view, the lattice basis can be used in any scattering calculations on the same footing as a conventional discrete $L_2$ basis like the harmonic oscillator basis or the basis of Gaussians. Since the basis functions are step-like functions in momentum space, the momentum dependence of all functions expressed via such a basis has also a histogram-like form.

## 2.4 Construction of WP states for the total Hamiltonian

Free WPs can be used as a basis to construct scattering WPs for the total Hamiltonian $h$ as its pseudostates. For this purpose, one applies a diagonalization procedure to the total Hamiltonian matrix in a free WP basis. As a result, one gets a discrete sets of eigenvalues $E_k$ and respective eigenvectors $|\tilde{z}_k\rangle$.

By such a diagonalization procedure, one derives a very convenient discrete representation for the scattering WPs as a superposition of free WPs:

$$|z_k\rangle \approx |\tilde{z}_k\rangle = \sum_{i=1}^{N} O_{ki}|x_i\rangle. \tag{7}$$

As it has been mentioned above, there is no restriction that $v$ should be a short-range potential. So that, this procedure can be applied even for the long-range Coulomb

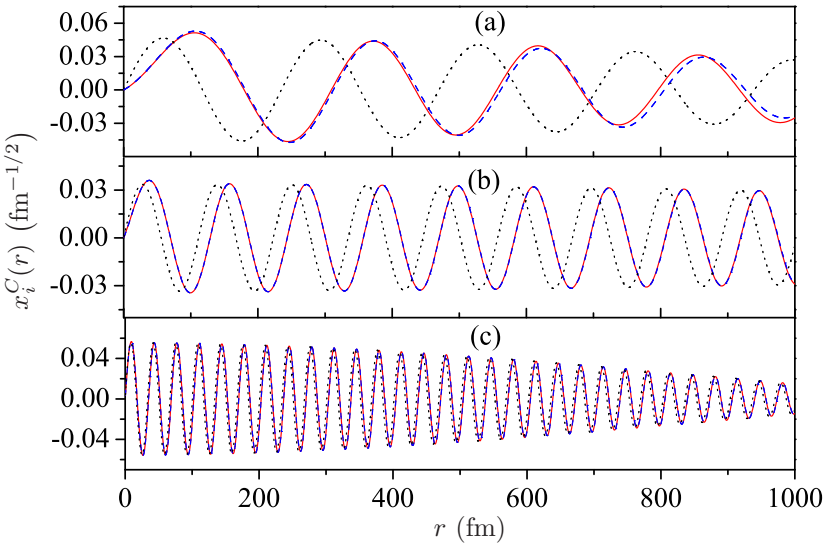


Figure 1: The exact $S$-wave Coulomb WPs (dashed curves), the pseudostates found via the free WP basis (solid curves) and the free WPs at the same energy (dotted curves) for $pp$ system at three center of mass energies: $E_{\text{c.m.}} = 0.03$ MeV (a), $E_{\text{c.m.}} = 0.133$ MeV (b) and $E_{\text{c.m.}} = 1.474$ MeV (c). In the case (c) the Coulomb phase shift is rather small, hence the respective three curves are very close to each other.

interaction. This statement is illustrated in Fig. 1 where the exact Coulomb WPs for $pp$ system are compared with the respective Coulomb pseudostates found by the diagonalization of the Coulomb Hamiltonian $h_C$ on the free WP basis, and the free WPs themselves at the same energy. It is clearly seen from the Figure the Coulomb WP $|x_i^C\rangle$ can be very accurately approximated by free WPs.

The pseudostate approximation (7) for the scattering WPs is extremely useful for few-body scattering studies where one is able to build a few- and many-body WP basis not only for a free motion Hamiltonian but also for a few-body channel Hamiltonian.

# 3 Solving scattering problems without equations

## 3.1 Discrete spectral shift function formalism

The discrete representation for scattering theory objects opens new possibilities in practical solving scattering problems. Below we briefly report the method based on the spectral shift function formalism, which allows to the find multichannel scattering matrix using spectral properties of the free and total Hamiltonian only [10].

The spectral shift function (SSF) $\xi(E) \equiv \xi(E; h, h_0)$ is an important object in the general spectral theory of perturbations which defines a spectral difference for two Hermitian operators $h_0$ and $h = h_0 + v$ (e. g., free and total Hamiltonians) in the discrete and continuous parts of the entire spectrum [17, 18]. This fact is known as the trace formula:

$$\mathrm{Tr}\,[f(h) - f(h_0)] = \int \mathrm{d}E\, f(E)\, \xi(E). \tag{8}$$

Here $f$ is some function and $\xi$ does not depend on $f$ but depends on two operators $h$ and $h_0$ only. Although $v$ is called *a perturbation* there is no restriction that it should be small. It is only assumed that the operator $v$ has a finite trace.

The most essential result of the SSF formalism for physical applications is the famous Birman–Krein formula [17], which relates the SSF with the determinant of the scattering operator $S$:

$$\det S(E) = \exp\bigl(-2\pi i\xi(E)\bigr). \tag{9}$$

In the single-channel scattering (e. g., at a fixed angular momentum), this formula implies that the SSF is equal up to a factor of $-\pi$ to a partial phase shift, $\delta(E) = -\pi\xi(E)$.

Let us add that, at negative energies, the SSF is a counting function which changes by one unit when crossing each bound state energy [10].

To define the SSF in a discretized representation, one has to use a concept of quasi-continuous spectrum introduced by I. M. Lifshitz [19] (see also details in ref. [10]). He considered a family of Hermitian operators $\{h_0^{(\alpha)}\}$ each depending on a small parameter $\alpha$ and having a purely discrete spectrum of eigenvalues (EVs) $\{E_j^0(\alpha)\}$ which can be approximated by a single continuous monotonic function $w(u)$:

$$\begin{aligned} &E_j^0(\alpha) = w(j\alpha) + O(\alpha), \\ &D_j^{(\alpha)} = E_{j+1}^0(\alpha) - E_j^0(\alpha) = \alpha\left[\left.\frac{\mathrm{d}w}{\mathrm{d}u}\right|_{u=j\alpha} + O(\alpha)\right]. \end{aligned} \tag{10}$$

All differences $D_j^{(\alpha)}$ decrease as $\alpha$ decreases and the quasi-continuous spectrum becomes more and more dense. Thus, in the limit $\alpha \to 0$, one has the limiting operator $h_0$ with a continuous spectrum. By adding the perturbation $v$ to $h_0^{(\alpha)}$ operators, one gets a family of total Hamiltonians $h^{(\alpha)}$ with shifted EVs $\{E_j(\alpha)\}$. One or several EVs of the perturbed spectrum may occur to be below the threshold and thus correspond to the bound states of $h$ while the rest belong to the quasi-continuous spectrum of this operator. Lifshitz has shown that the following relation between perturbed and unperturbed EVs in quasi-continuous spectrum takes place [10, 19]:

$$E_j(\alpha) = E_j^0(\alpha) + D_j^{(\alpha)}\xi_j + o(\alpha), \tag{11}$$

where $D_j^{(\alpha)}$ is defined in Eq. (10) and $\xi_j = \xi\bigl(E_j(\alpha)\bigr)$ is the spectral shift function defined at discrete energy values. The formula (11) is the basic for the Discrete Spectral Shift (DSS) method. It results in a very simple approximate expression for the partial phase shift:

$$\delta(E_j^0) = -\pi\xi(E_j^0) \approx -\pi\frac{E_j - E_j^0}{D_j}. \tag{12}$$

This method may be applied to any continuum discretization procedure, e. g., when one considers a particle scattering in a box and the box size $R$ is increased to infinity ($\alpha \sim \frac{1}{R}$) [10]. Another useful case is the solution of the scattering problem in some finite $L_2$ basis when the parameter $\alpha$ is decreasing with increasing the basis dimension $N$ [10].

It should be stressed that the above result is related to other methods which allow to find phase shifts without solving the scattering equations. It is worth to mention

here the Lüsher approach which is widely used in low energy EFT applications [14]. Recently the SS-HORSE method has been developed [15,16] which can be treated as a SSF formalism in the Harmonic Oscillator representation.

### 3.2 New treatment of multichannel pseudostates

In a multichannel case, the total Hamiltonian can be written in a matrix form as

$$h_{\nu\nu'} = h_0^{\nu}\,\delta_{\nu\nu'} + v_{\nu\nu'}, \qquad \nu,\nu' = 1,\dots,d, \tag{13}$$

where $\nu$ is a channel index, $h_0^{\nu}$ are the channel unperturbed Hamiltonians and $v_{\nu\nu'}$ are coupling potentials.

The trace (8) and Birman–Krein (9) formulas are valid in the multichannel case as well. However they correspond to the total spectral density of the matrix Hamiltonian $\mathbf{h}$ from Eq. (13) and cannot be used for separate calculations of elastic and inelastic amplitudes in different channels. In particular, the spectral shift function at each energy is just a sum of all *eigenphases* [10].

Nevertheless, we have shown that Eq. (12) can be generalized to evaluate separate eigenphases from the differences of free and total Hamiltonian eigenvalues [10] similarly to the single-channel case. Here each EV of the discretized spectrum $\{E_j^0\}$ of the multichannel free Hamiltonian $\mathbf{h}_0$ should be degenerate with the multiplicity $d$ equal to the number of open channels at the given energy. An inclusion of a channel-coupling interaction leads to the splitting of the above multiple energy levels. Finally, the spectrum of the total multichannel Hamiltonian $\mathbf{h}$ consists of serieses of eigenvalues $\{E_j^{\varkappa}\}_{\varkappa=1}^{d}$ for each $j$ (here $\varkappa$ is the eigenchannel index) arising from the initial unperturbed eigenvalues $E_j^0$ (see Ref. [10] for the details). This effect is illustrated in Fig. 2 for a two-channel problem.

Thus a diagonalization of the total Hamiltonian (13) matrix in the coupled-channel free WP basis $\{|x_i^{\nu}\rangle\}_{\nu=1}^{d}$ results in a set of pseudostates $|z_k^{\varkappa}\rangle$ with EVs $E_k^{\varkappa}$ expanded in a series of free WP states:

$$|z_k^{\varkappa}\rangle = \sum_{\nu,i} O_{ki}^{\varkappa\nu}\,|x_i^{\nu}\rangle. \tag{14}$$

These pseudostates can be treated as approximations for the multichannel WPs of the total Hamiltonian $\mathbf{h}$ [7].

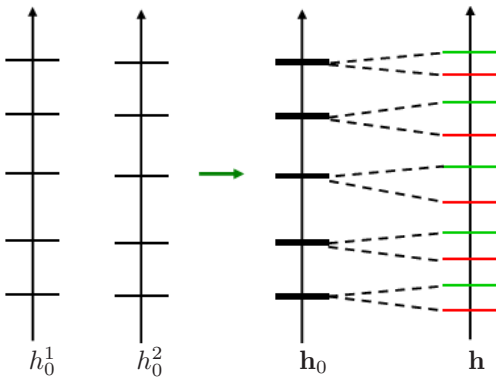


Figure 2: The splitting effect caused by the inclusion of the coupled-channel interaction $\mathbf{v}$: the similar eigenvalues of free Hamiltonians $h_0^1$ and $h_0^2$ form discretized spectrum of the matrix free Hamiltonian $\mathbf{h}_0$ with degenerated energy levels each splitted into a pair of levels (shown with different colors) of the total Hamiltonian $\mathbf{h}$.

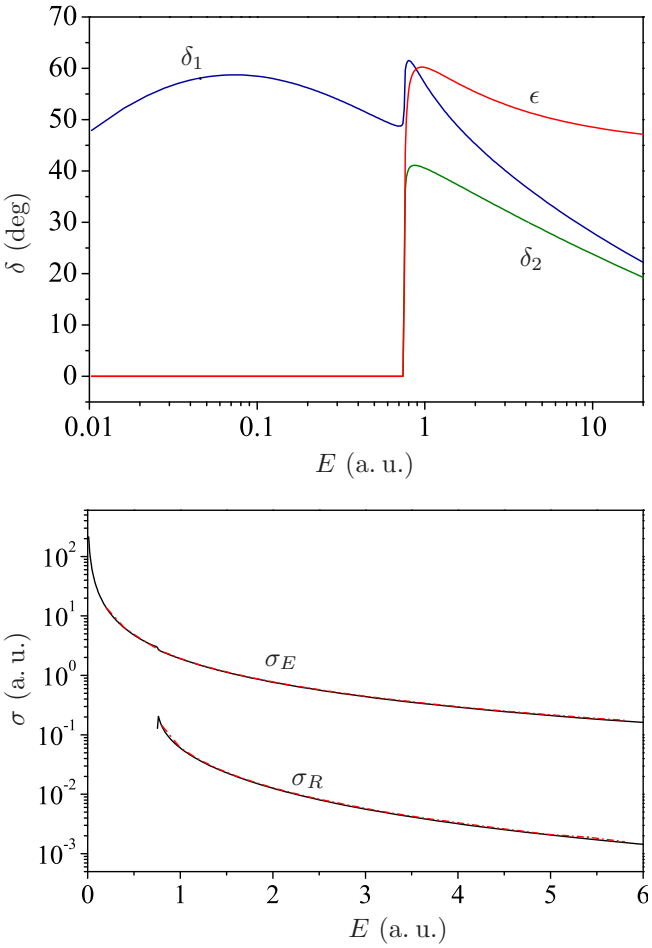


Figure 3: Eigenphases $\delta_{1,2}$ and mixing angle $\epsilon$ (top) together with elastic and reaction cross sections (bottom) found via the DSS method for the two-channel $e-$H scattering (solid curves). The dash-dotted curves (almost indistinguishable from the solid ones) in the bottom panel present the results of Ref. [20].

Then one can define different spectral shift functions in the eigenchannel representation (each for a separate eigenchannel) and relate them to the eigenphases of the multichannel problem. Finally, these eigenphases are defined again through the discrete spectral shifts:

$$\delta_\varkappa(E_j^0) \approx -\pi \frac{E_j^\varkappa - E_j^0}{D_j}, \quad \varkappa = 1, \dots, d, \tag{15}$$

where $E_j^0$ is the eigenvalue of the free Hamiltonian $\mathbf{h}_0$ with the multiplicity $d$, $E_j^\varkappa$ is the eigenvalue of the total Hamiltonian $\mathbf{h}$, and $D_j$ is the energy width of the corresponding discretization interval of $\mathbf{h}_0$.

Our results for the model two-channel $e-$H scattering problem obtained in the DSS approach are shown in Fig. 3 in comparison with the results of Ref. [20]. A coupled-channel potential including $1S-2S$ excitation of the hydrogen atom has been used in these calculations. The parameters of the model interaction has been taken from Ref. [20]. It is seen that the DSS technique reproduces the reaction cross section very well in a wide energy region except only for one or two energy points just near the threshold of the second channel.

A detailed description of the DSS approach and various numerical examples of single- and multi-channel scattering applications, including those with non-local and complex-valued potentials, can be found in Refs. [10].

### 3.3 Off-shell multichannel *t*-matrix from the diagonalization

With the treatment of the multichannel pseudostates as shown above, a finite-dimensional representation for the total resolvent takes a diagonal form in the multichannel case [7]:

$$g(E) \approx \sum_{n=1}^{N_b} \frac{|\psi_n\rangle\langle\psi_n|}{E - E_n} + \sum_{\varkappa=1}^{d} \sum_{k=1}^{N_\varkappa} |z_k^\varkappa\rangle \, g_k^\varkappa(E) \, \langle z_k^\varkappa|, \tag{16}$$

which is similar to the single-channel total resolvent (5). It should be stressed that the above expansion does not represent the pole-like pseudostate approximation for the total resolvent but it corresponds to the diagonalization of the coupled-channel continuous spectrum of the total Hamiltonian within the scattering wave-packet formalism.

Next, substituting the total resolvent by its representation (16) in the explicit formula for the transition operator,

$$t(E) = v + v \, g(E) \, v, \tag{17}$$

one obtaines the off-shell multichannel $t$-matrix as the following matrix element in the channel free WP basis:

$$t_{\nu\nu'}(E; p, p') \sim \langle x_i^\nu | t(E) | x_{i'}^{\nu'} \rangle, \quad p \in \mathfrak{D}_i, \quad p' \in \mathfrak{D}_{i'}. \tag{18}$$

Thus this technique makes it possible to find the off-shell $t$-matrix for a multichannel scattering problem by a one-fold diagonalization of the total Hamiltonian matrix in free WP basis for any energy $E$. Here, at all required energy points, the same set of pseudostates $|z_k^\varkappa\rangle$ should be used and only the eigenvalues $g_k^\varkappa(E)$ must be recalculated which is very simple.

As an example of an application of the diagonalization procedure to the calculation of the $NN$ scattering amplitudes, we present in Fig. 4 the partial phase shifts for the coupled ${}^3S_1 - {}^3D_1$ spin-triplet channels supported by the CD-Bonn $NN$ potential [21]. To check the accuracy of the approach, we compare in this figure the results of the direct numerical solution for the integral Lippmann–Schwinger equation with the results of a single diagonalization for the respective $NN$ coupled-channel Hamiltonian in a very broad interval of laboratory energies $E_{\rm lab}$ from zero up to 800 MeV. The dimensionality of the free WP bases for these calculations is $N = 100$ in each partial wave. As the discretization mesh, we used here the Chebyshev grid (see details in Ref. [7]). It is clearly seen that the results for the direct and diagonalization solutions are nearly indistinguishable in the whole energy region studied.

It should be mentioned that the proposed diagonalization technique is useful for solving scattering problems in medium as well. Very recently [22], we have generalized this approach to solving the Bethe–Goldstone equation for the reaction matrix in infinite nuclear matter.

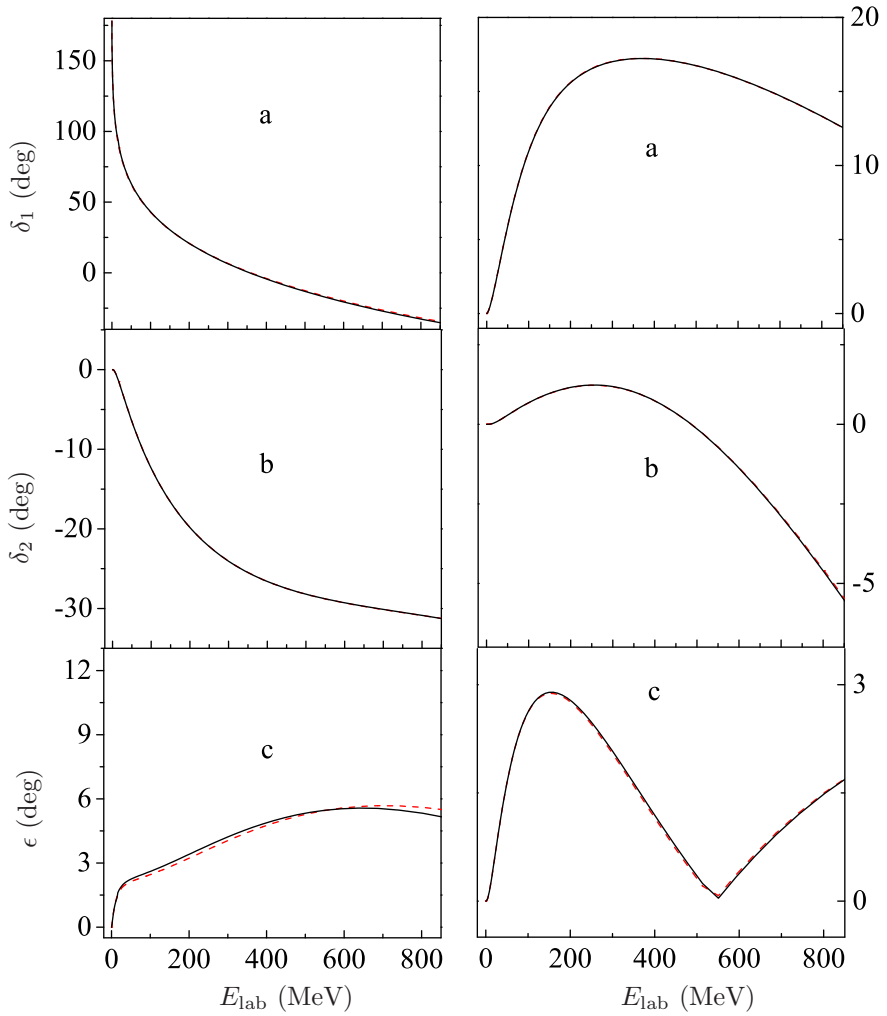


Figure 4: Partial phase shifts $\delta_1$ (a), $\delta_2$ (b) and mixing angle $\varepsilon$ (c) for the coupled spin-triplet ${}^3S_1{-}{}^3D_1$ (left) and ${}^3P_2{-}{}^3F_2$ (right) channels of $NN$ scattering calculated using the CD-Bonn $NN$ potential (solid curves) in comparison with the results of a direct numerical solution of the respective Lippmann–Schwinger equation (dashed curves).

## 4 Few-body scattering problem in the momentum lattice basis

It has been shown above that the diagonalization procedure for the total Hamiltonian in the free WP basis allows to find on-shell or off-shell quantities for problems in continuum in a wide energy region without solving scattering equations. However a generalization of this approach to the three- and few-body cases is not straightforward due to a complexity of the few-body continuum and corresponding boundary conditions.

For the studies of the few-body scattering, we have developed a closed formalism based on the free WP basis (the momentum lattice basis) which allows to find matrix analogs of the integral scattering theory equations and to solve them efficiently. We start below from a general description of this formalism in the two-body case.

## 4.1 Discrete version of scattering theory

Within the WP lattice formalism, a three-step discretization procedure is introduced:

(i) Division of continuous spectrum of the free Hamiltonian into non-overlapping intervals and introduction of the free WPs.

(ii) Projection of the scattering (as well as bound-state) wave functions and operators onto the above WP space.

(iii) Additional energy averaging of energy-dependent operators.

The last item means that one should apply the energy-averaging procedure, e. g., to the finite-dimensional representation (5) of the free resolvent $g_0(E) = [E + \mathrm{i}0 - h_0]^{-1}$,

$$\mathfrak{g}(E) \to \mathfrak{g}_0^k = \frac{1}{D_k} \int_{\mathfrak{D}_k} \mathfrak{g}_0(E)\, dE, \tag{19}$$

where $D_k = \mathcal{E}_k - \mathcal{E}_{k-1}$ is an energy width of the interval $\mathfrak{D}_k$. This averaging makes it possible to avoid logarithmic singularities at the end-points of the energy intervals which are inherent in the matrix elements $g_k(E)$ in Eq. (5) and allows also to accomplish a complete discretization of the solution scheme [7].

It would be useful to demonstrate how the above discretization procedure works in practical applications by solving the Lippmann–Schwinger equation for the transition operator $t(E)$:

$$t(E) = v + v\, g_0(E)\, t(E). \tag{20}$$

Applying the above three steps (i)–(iii), one gets a discrete set of operators $\mathfrak{t}^k$ at $E \in \mathfrak{D}_k$ (instead of the operator $t(E)$ continuously dependent on energy). The matrix elements of $\mathfrak{t}^k$ in the WP basis are related directly to the off-shell elements of the $t$-matrix:

$$t(p, p', E) \approx \frac{[\mathfrak{t}^k]_{ij}}{\sqrt{D_i D_j}}, \qquad \begin{pmatrix} p \in \mathfrak{D}_i \\ p' \in \mathfrak{D}_j \\ E \in \mathfrak{D}_k \end{pmatrix}. \tag{21}$$

These operators $\mathfrak{t}^k$ satisfy simple matrix equations

$$\mathfrak{t}^k = \mathfrak{v} + \mathfrak{v}\, \mathfrak{g}_0^k\, \mathfrak{t}^k, \qquad E \in \mathfrak{D}_k, \tag{22}$$

where the gothic letters denote the WP projections of the respective operators. Using Eq. (22), one can obtain any of on- and off-shell $t$-matrix elements whose energy and momentum dependencies are represented by histograms. It should be emphasized that the $t$-matrix constructed in the WP representation satisfies exactly the unitarity relation [7].

Finally, the $S$-matrix (and the partial phase shifts) can be found by means of the relation

$$S(E) \approx 1 - 2\pi i \frac{[\mathfrak{t}^k]_{kk}}{D_k}, \qquad E \in \mathfrak{D}_k. \tag{23}$$

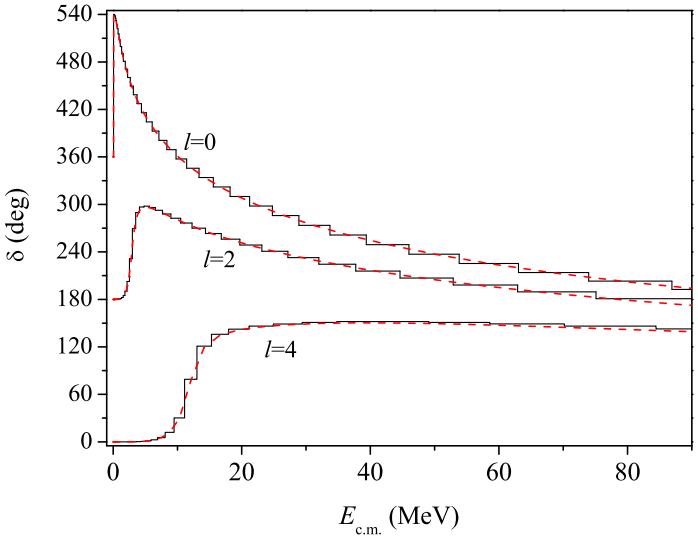


Figure 5: $S$, $D$ and $G$ partial phase shifts of $\alpha-\alpha$ scattering obtained via the WP approach (solid curves) and by a direct numerical integration of the Schrödinger equation using the Numerov method (dashed curves).

As an illustration of accuracy of this fully-discretized technique for calculating the transition operator, we present here the solution of the $\alpha-\alpha$ scattering problem with interaction including both nuclear and Coulomb potentials [7]. The basic $S$, $D$ and $G$ partial $\alpha-\alpha$ phase shifts obtained using the above WP technique with the additional energy averaging are displayed in Fig. 5. Here the Coulomb WPs are used as a basis.

## 4.2 Wave-packet basis in few-body case

If a few-body Hamiltonian can be written in the form of a direct sum of two-body ones,

$$H_M = h_1 \oplus h_2 \oplus ... \oplus h_M, \tag{24}$$

the WP basis states for $H_M$ can be constructed straightforwardly as direct products of the two-body ones:

$$|Z_{i_1 i_2 ... i_M}\rangle = |z_{i_1}\rangle \otimes |\bar{z}_{i_2}\rangle \otimes \ldots \otimes |\bar{\bar{z}}_{i_M}\rangle, \tag{25}$$

where we use bars above the $z$-functions to distinguish states corresponding to different subsystems. In the basis (25), the matrix of the Hamiltonian $H_M$ is diagonal and the matrix of the resolvent $G_M(E) = [E + i0 - H_M]^{-1}$ has also an explicit diagonal form.

In the studies of scattering in a system of three identical particles, 1, 2 and 3, useful examples of Hamiltonians of the type (24) are the free Hamiltonian,

$$H_0 = h_{0p} \oplus h_{0q}, \tag{26}$$

and the channel Hamiltonian,

$$H_1 = (h_{0p} + v_1) \oplus h_{0q}, \tag{27}$$

defined for a given Jacobi partition (e. g., $\{23\}1$) with momenta $(p, q)$, where $h_{0p}$ and $h_{0q}$ are the kinetic energy operators and $v_1$ is the interaction between the particles 2 and 3. One can introduce the free WP states $|X_{ij}^{\gamma}\rangle$ and the channel WP

states $|Z_{kj}^{\gamma}\rangle$ using the two-body ones (with an account of the necessary spin-angular parts labeled by quantum numbers $\gamma$) and relate the latter to the former by a simple rotation [7] (all necessary quantum numbers should be taken into account):

$$|Z_{kj}^{\gamma}\rangle = \sum_{\gamma',i} O_{ki}^{\gamma\gamma'} |X_{ij}^{\gamma'}\rangle. \tag{28}$$

This channel basis construction scheme can be also generalized to the charged particle case [7].

### 4.3 Solution of Faddeev equation for *nd* problem in the discrete representation

Here we discuss briefly the solving of Faddeev equations for a scattering of three identical particles 1, 2 and 3 with mass $m$ (nucleons). In this case, elastic scattering observables can be obtained from a single Faddeev equation for the transition operator $\bar{U}$ (the so-called AGS equation), e. g., in the following form [23]:

$$\bar{U} = PG_0^{-1} + PtG_0\bar{U}, \tag{29}$$

where $t$ is the two-body off-shell $t$-matrix in three-body space, $G_0 = (E + i0 - H_0)^{-1}$ is the free three-body resolvent and $P$ is the permutation operator which changes the momentum variables from one Jacobi set to another. In the case of three identical particles, the operator $P$ is defined as a sum of two cyclic permutations:

$$P = P_{12}P_{23} + P_{13}P_{23}. \tag{30}$$

It should be emphasized that a similar permutation operator is included in the kernels of Faddeev equations in the case of non-identical particles.

We have shown [7] that one can rewrite Eq. (29) in the equivalent half-shell form,

$$U = Pv_1 + Pv_1G_1U, \tag{31}$$

where $v_1$ is the two-body interaction and $G_1(E) = [E + \mathrm{i}0 - H_1]^{-1}$ is the resolvent of the channel Hamiltonian (27).

By projecting the integral equation (31) onto the channel WP basis (28), one derives the matrix equation

$$\mathbb{U} = \mathbb{P}\mathbb{V}_1 + \mathbb{P}\mathbb{V}_1\mathbb{G}_1\mathbb{U}. \tag{32}$$

Here $\mathbb{V}_1$ and $\mathbb{G}_1$ are the matrices of the pairwise interaction and of the channel resolvent, respectively, which matrix elements can be found in an explicit form.

Thus, to obtain the elastic scattering amplitude, it is required 1) to calculate the matrix elements of matrices $\mathbb{P}$, $\mathbb{V}_1$, $\mathbb{G}_1$ and 2) to solve the system of algebraic equations (32).

The matrix $\mathbb{V}_1$ of the potential $v_1$ is diagonal in the indices of the wave-packet basis corresponding to the Jacobi coordinate $q$ and thus has a block form. Its matrix in the channel WP basis is defined with the help of interaction matrix $\mathbb{V}_1^0$ in the free WP basis and the rotation matrix $\mathbb{O}$.

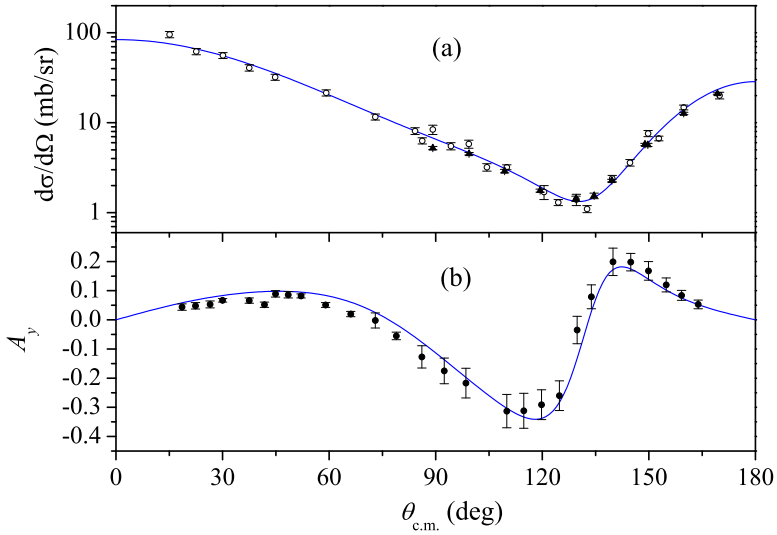


Figure 6: Elastic $nd$ scattering differential cross section (a) and neutron vector analyzing power $A_y$ (b) at 35 MeV obtained within the WP approach (solid curves). Experiment: $pd$ data at 35 MeV [25] (filled circles), $nd$ data at 36 MeV [26] (empty circles), $nd$ data 35 MeV [27] (triangles).

The matrix of the operator $P$ in the three-body lattice basis corresponds to the overlap of basis functions defined in different Jacobi sets:

$$[\mathbb{P}^0]^{\gamma,\gamma'}_{ij,i'j'} \equiv \langle X^{\gamma}_{ij}|P|X^{\gamma'}_{i'j'}\rangle. \tag{33}$$

Such matrix elements are calculated by integration over the basis functions in momentum space (see details in Refs. [8, 9]). Thus, we have rather simple formulas and respective numerical algorithms to determine all quantities entering the kernel of the matrix Faddeev equation (32).

The elastic on-shell amplitude in the wave-packet representation is calculated as a diagonal (on-shell) matrix element of the $\mathbb{U}$-matrix [7] while the breakup amplitudes can be found from off-diagonal elements of the same matrix.

The differential cross sections of the $nd$ elastic scattering and the neutron vector analyzing power $A_y$ calculated using the realistic Nijmegen I $NN$ potential [24] in the WP approach at 35 MeV are presented in Fig. 6 in comparison with the experimental data. It is evident from the figure that the agreement with the data is rather well. Here the WP basis of the dimensionality over the discretized $p$ and $q$ momenta of $N \times \bar{N} = 100 \times 100$ has been used and the partial waves with the total angular momentum up to $J \leq 17/2$ have been taken into account.

# 5 Solving by GPU

## 5.1 Details of numerical scheme for solving Faddeev equation in the discrete representation

As shown above, we have reduced the integral Faddeev equation (31) to the matrix equation (32). As a result, the conventional difficulties of solving the integral equa-

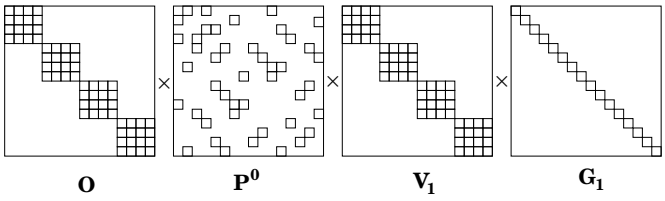


Figure 7: The structure of matrix kernel (34) of the Faddeev equation (32): nonzero elements are marked by squares.

tion (29) are avoided, however the price to be paid is a high dimensionality of the resulting system of algebraic equations.

In fact, we have found [7] that quite satisfactory results can be obtained with a basis size for each Jacobi momentum $N \sim \bar{N} \sim 100{-}150$. This means that even in the simplest single-channel case when all quantum numbers in the set $\gamma$ are conserved (e. g., for spin-quartet $S$-wave three-fermion scattering or $S$-wave three-boson scattering), one gets a kernel matrix of the dimensionality $M = N \times \bar{N} \sim 10000{-}20000$. In the case of a realistic three-body scattering, it is necessary to include many spin-angular channels (up to 62 channels in the case of three-nucleon system) and therefore the dimensionality of the kernel matrix increases up to $5 \cdot 10^5{-}10^6$. It is clear that the kernel matrix of this size cannot be stored in the RAM of an ordinary PC.

However a specific matrix structure of the kernel of Eq. (32) makes it possible to overcome this difficulty and to eliminate completely the need for the external memory. Indeed, the matrix kernel $\mathbb{K}$ in Eq. (32) can be written as a product of four matrices,

$$\mathbb{K} = \mathbb{P}\mathbb{V}_1\mathbb{G}_1 \equiv \mathbb{O}\mathbb{P}^0\tilde{\mathbb{V}}_1\mathbb{G}_1, \tag{34}$$

where $\tilde{\mathbb{V}}_1 = \mathbb{O}^{\mathrm{T}}\mathbb{V}_1$. Here $\mathbb{G}_1$ is a diagonal matrix, $\mathbb{P}^0$ is the permutation matrix of a high sparsity, while $\tilde{\mathbb{V}}_1$ and $\mathbb{O}$ are block matrices comprising identical blocks of the dimensionality $N$ (see Fig. 7).

The problem of the high dimensionality is resolved by storing only the individual multipliers of the matrix kernel $\mathbb{K}$ in RAM. Moreover, one can store the highly sparse matrix $\mathbb{P}^0$ in a compressed form (i. e., only its nonzero elements), then the complete set of data required for the iteration process can be placed in RAM. Although three extra matrix multiplication is added at each iteration step in this case, the computer time spent on iterations is reduced more than 10 times as compared to the procedure employing the external memory.

Thus our overall numerical scheme includes the following main steps:

1. Processing of the input data.
2. Calculation of nonzero elements of the permutation matrix $\mathbb{P}^0$.
3. Calculation of the channel resolvent matrix $\mathbb{G}_1$.
4. Iterations of the matrix equation (32) and finding its solution using the Padé approximant technique.

The runtimes for the steps 1 and 3 are practically negligible in comparison with the total running time, while the execution of the step 4 — finding the solution of the matrix system by iterations — takes about 20% of the total time needed for a single-thread computing of the whole problem. Hence we shall discuss below an optimization

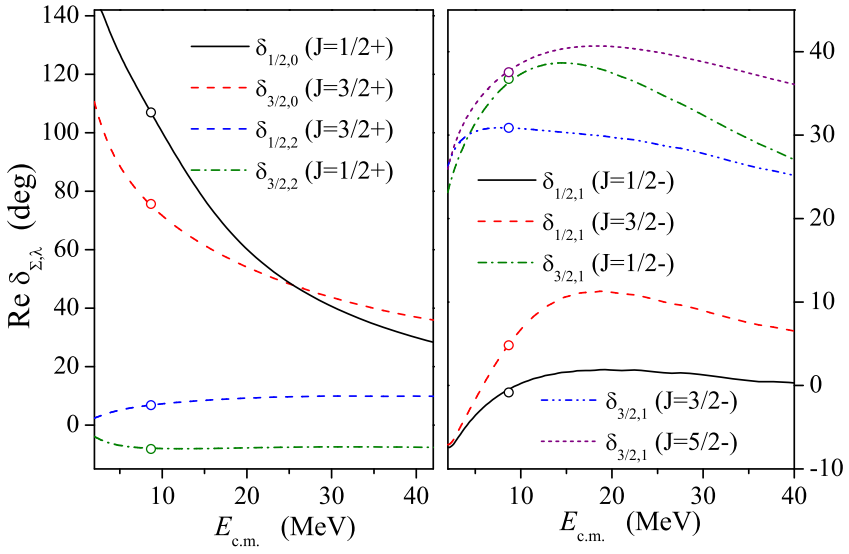


Figure 8: Some of $S$, $D$ and $P$ partial phase shifts of the elastic $nd$ scattering obtained within the WP approach (solid curves) and within the standard Faddeev calculations (circles) [23].

of the step 2 only, viz. the calculation of the matrix $\mathbb{P}^0$ elements. Since all these elements are calculated using the same code and are completely independent from each other, the algorithm seems to be suitable for a parallelization and implementation on multiprocessor systems like GPU. However, since the matrix $\mathbb{P}^0$ is of a high sparsity, we have developed a special technique in order to get an essential acceleration due to the GPU realization. In particular, we apply an additional *pre-selection* of the nonzero $\mathbb{P}^0$ matrix elements.

It should be emphasized that the steps 1 and 2 do not depend on the incident energy. The current energy is taken into account only at steps 3 and 4 when one calculates the channel resolvent matrix elements and solves the matrix equation for the scattering amplitude. Therefore, if one needs to calculate the scattering observables in a wide energy region, the whole computing time is not increasing essentially because the most time-consuming part of the code (step 2) is carried out only once for many energy points.

Various even- and odd-parity partial phase shifts of the elastic $nd$ scattering calculated with the Nijmegen I $NN$ potential via the proposed WP approach are presented in a wide energy region in Fig. 8. The same permutation matrix has been used to derive all these results.

## 5.2 GPU acceleration for the *nd* scattering problem with *s*-wave *NN* potential

There is a number of issues associated with the organization of the data transfer between the RAM and GPU and also with the GPU computation itself which makes highly nontrivial the GPU realization in this case. These issues impose severe restrictions on the acceleration due to the GPU realization. One can define the GPU

acceleration $\eta$ as a ratio of the single-thread CPU computation runtime to the multithread GPU computation runtime:

$$\eta = t_{\mathrm{CPU}}/t_{\mathrm{GPU}}. \tag{35}$$

This acceleration depends on the ratio of the actual time for the calculation of a single matrix element $t_0$ to the time of transmitting the result from the GPU back to the RAM $T$, on the number of GPU cores $N_{\mathrm{c}}$ and their speed $r_{\mathrm{GPU}}$ compared to the speed of the CPU core $r_{\mathrm{CPU}}$, and also on the dimension of the matrix $M$:

$$\eta = f\left(\frac{t_0}{T}, N_{\mathrm{c}}, r_{\mathrm{GPU}}, r_{\mathrm{CPU}}, M\right). \tag{36}$$

Figure 9 shows the dependence of the CPU and GPU computing times as well as the GPU acceleration $\eta$ in calculation of the permutation matrix on its total dimensionality $M = N \times \bar{N}$ (for $N = \bar{N}$) in the case of the $s$-wave $NN$ interaction MT III. In this calculation, the GPU code was executed with 65 536 threads. For the comparison, we display in this figure also the CPU and GPU times needed for the pre-selection of nonzero matrix elements. It is clear from the figure that one needs to use the GPU not only for the calculation of nonzero elements which takes most of the time in the single-thread CPU computing, but also for the pre-selection of nonzero matrix elements to achieve an essential acceleration.

It is seen that the runtime for the calculation of the $\mathbb{P}^0$ nonzero elements which takes the main fraction of the CPU computing time, is reduced by more than 100 times. The total GPU acceleration in calculating the $S$-wave partial phase shifts reaches 50. As a result of all these innovations, the total three-body scattering calculation takes only 7 sec on an ordinary PC with GPU.

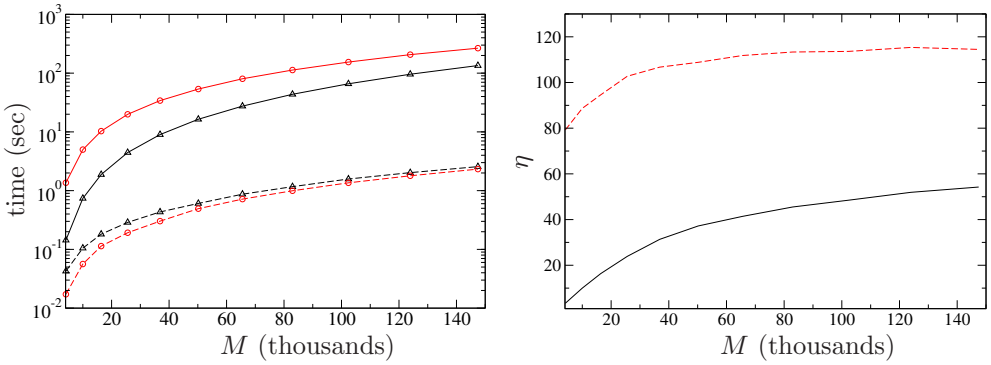


Figure 9: Left: the CPU (solid curves) and GPU (dashed curves) computing times for the pre-selection (triangles) and calculation of the $\mathbb{P}^0$ nonzero elements (circles) in the case of $s$-wave $NN$ interaction. Right: the GPU acceleration $\eta$ for calculation of the permutation matrix (dashed curve) and for the complete solution of the $S$-wave $nd$ scattering problem (solid curve). Here $M$ is the total basis dimensionality.

### 5.3 GPU acceleration in the *nd* scattering problem with realistic *NN* potential

Unlike the simplest single-channel *nd* scattering discussed above, in the case of realistic $NN$ interactions, we have many coupled spin-angular channels (up to 62 channels if the total angular momentum in $NN$ pairs is restricted to $j \leq 3$). In this case, the calculation of each element of the permutation matrix $\mathbb{P}^0$ comprises numerical calculations of several tens of double numerical integrals containing Legendre polynomials.

Figure 10 demonstrates the GPU acceleration $\eta$ versus the total basis dimensionality $M$ in the solution of 18-channel Faddeev equation for the partial three-body elastic amplitude with the total angular momentum $J = \frac{1}{2}^+$ in the case of realistic Nijmegen I $NN$ interaction. The dashed and dash-dotted curves present the GPU acceleration at the stages of the pre-selection of nonzero elements of the permutation matrix $\mathbb{P}^0$ and of calculation of these elements, respectively.

From these results, it is evident that the acceleration for calculating the large coupled-channel permutation matrix is about 15 times that is considerably smaller than in the above single-channel case. Nevertheless, switching from the CPU to the GPU realization *on the same PC* makes it possible to obtain a quite impressive acceleration of about 10 times in the solution of the 18-channel scattering problem.

In realistic calculations of the observables of elastic three-body scattering, it is necessary to include up to 62 spin-orbital channels. For the current numerical scheme, the efficiency of the GPU optimization decreases with increasing the number of channels. As is shown in Ref. [9], the time of calculations of the permutation matrix elements is decreased by 8.7 times only due to the GPU optimization. Moreover, in this case,

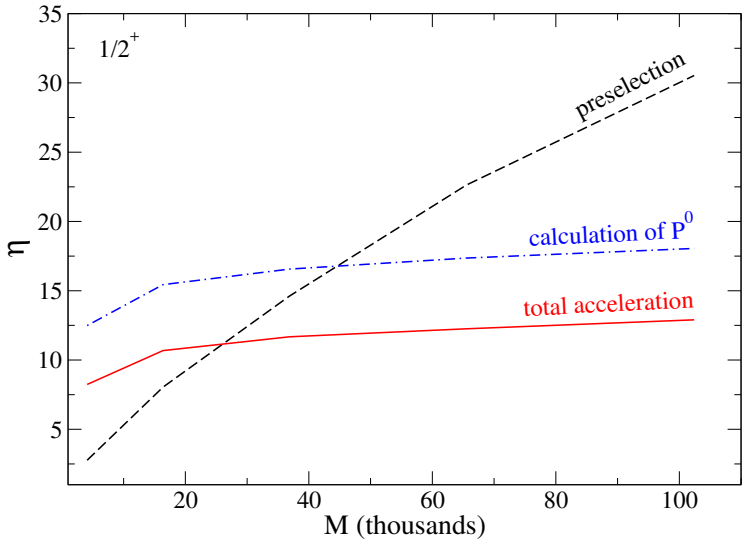


Figure 10: Dependence of the GPU acceleration $\eta$ on the dimensionality of the basis $M$ for the *nd* scattering problem with Nijmegen I $NN$ potential at $J = \frac{1}{2}^+$: dashed curve — acceleration for the pre-selection of nonzero elements in the permutation matrix $\mathbb{P}^0$, dash-dotted curve — acceleration for the calculation of these nonzero elements, solid curve — acceleration of the complete solution.

the major fraction of the computational time is spent not on the permutation matrix but on the successive iterations of the very large matrix equation, i. e., on the final step 4. This step takes now about 69% of the total computational time; as a result, the total acceleration of the entire procedure is only 3.2. It should be stressed however that the current numerical scheme can be further optimized. We plan to parallelize the final step 4 in our next studies. It is also clear that the use of a more powerful specialized graphics processor like Tesla K80 would lead even to a considerably larger acceleration of the calculations.

# 6 Summary

We have described here a general technique for solving few-body scattering problems based on a complete continuum discretization and a projection of scattering operators and wave functions onto the basis of stationary wave packets. Due to the properties of the basis functions, the approach combines the advantages of the $L_2$-type techniques associated with calculations with normalized wave functions and, on the other hand, with the rigorous integral equation formalism of the scattering theory. As a result, such a WP projection makes it possible to transform complicated singular multi-dimensional integral equations like the Lippmann–Schwinger or Faddeev–Yakubovsky equations to regular matrix equations which can be solved directly within computational procedures similar to those used in the bound-state type calculations.

Moreover, it has been shown that the above computational procedures can be rather easily adapted to a parallel realization, in particular, they are suitable for processing on a desktop PC supplied with a GPU. Although we have found out that the acceleration achieved due to the GPU realization depends strongly on the dimensionality of the basis and on the complexity of the problem, e. g., on the number of spin-angular channels involved, the results obtained for the elastic $nd$ scattering problem with semi-realistic and realistic $NN$ potentials appear to be very promising for further investigations.

Let us note that the developed GPU-accelerated discrete approach for quantum scattering problems can be implemented in other areas of quantum physics, as well as in a number of important areas of classical physics involving the need to solve multidimensional problems for continuous media studies.

## Acknowledgments

The authors appreciate a partial financial support of the RFBR grants 16-02-00049, 16-02-00265 and joint RFBR-DFG grant 16-52-12005.

# References

[1] L. D. Faddeev, Sov. Phys. JETP **12**, 1014 (1961); O. A. Yakubovsky, Sov. J. Nucl. Phys. **5**, 937 (1967).

[2] V. D. Efros, W. Leidemann, G. Orlandini and E. L. Tomusiak, Phys. Rev. C **81**, 034001 (2010).

[3] E. Garrido, A. Kievsky, M. Viviani and Phys. Rev. C **90**, 014607 (2014).

[4] I. B. Abdurakhmanov, A. S. Kadyrov and I. Bray, Phys. Rev. A **94**, 022703 (2016).

[5] J. A. Lay, A. M. Moro, J. M. Arias and J. Gomez-Camacho, Phys. Rev. C **82**, 024605 (2010).

[6] J. Carbonell, A. Deltuva, A.C. Fonseca and R. Lazauskas, Prog. Part. Nucl. Phys. **74**, 55 (2014).

[7] O. A. Rubtsova, V. I. Kukulin and V. N. Pomerantsev, Ann. Phys. (NY) **360**, 613 (2015).

[8] V. N. Pomerantsev, V. I. Kukulin and O. A. Rubtsova, Phys. Rev. C **89**, 064008 (2014).

[9] V. N. Pomerantsev, V. I. Kukulin, O. A. Rubtsova and S. K. Sakhiev, Comput. Phys. Commun. **204**, 121 (2016).

[10] O. A. Rubtsova, V. I. Kukulin, V. N. Pomerantsev and A. Faessler, Phys. Rev. C **81**, 064003 (2010); O.A. Rubtsova, V. I. Kukulin and V. N. Pomerantsev, Phys. At. Nucl. **77**, 486 (2014).

[11] W. Greiner, *Quantum mechanics: An introduction, 4th ed.* Springer, 2001.

[12] N. K. Timifeyuk and R. C. Johnson, Phys. Rev. C **87**, 064610 (2013).

[13] M. Lüscher, Nucl. Phys. B **354**, 531 (1991).

[14] P. Guo, J. J. Dudek, R. G. Edwards and A. P. Szczepaniak, Phys. Rev. D **88**, 014501 (2013).

[15] A. M. Shirokov, A. I. Mazur, I. A. Mazur, J. P. Vary, Phys. Rev. C **94**, 064320 (2016).

[16] A. M. Shirokov, G. Papadimitriou, A. I. Mazur, I. A. Mazur, R. Roth and J. P. Vary, Phys. Rev. Lett. **117**, 182502 (2016).

[17] D. R. Yafaev, *Mathematical scattering theory: General theory.* Amer. Math. Soc., Providence, RI, 1992.

[18] M. S. Birman and A. B. Pushnitsky, Integr. Equ. Oper. Theory **30**, 191 (1998).

[19] I. M. Lifshitz, Zh. Eksp. Teor. Fiz. **17**, 1076 (1947) (*in Russian*).

[20] B. H. Brandsen and A. T. Stelbovics, J. Phys. B **17**, 1874 (1984).

[21] R. Machleidt, F. Sammarruca and Y. Song, Phys. Rev. C **53**, R1483 (1996).

[22] H. Müther, O. A. Rubtsova, V. I. Kukulin and V. N. Pomerantsev, Phys. Rev. C **94**, 024328 (2016).

[23] W. Glöckle, H. Witała, D. Hüber, H. Kamada, J. Golack, Phys. Rep. **274**, 107 (1996).

[24] V. G. J. Stoks, R. A. M. Klomp, C. P. F. Terheggen and J. J. de Swart, Phys. Rev. C **49**, 2950 (1994).

[25] S. N. Bunker, J. M. Cameron, R. F. Carlson, J. R. Richardson, P. Tomaš, W. T. H. Van Oers and J. W. Verba, Nucl. Phys. A **113**, 461 (1968).

[26] J. L. Romero, J. A. Jungerman, F. P. Brady, W. J. Knox and Y. Ishizaki, Phys. Rev. C **2**, 2134 (1970).

[27] F. P. Brady, W. B. Broste and J. C. Wang, Phys. Rev. C **9**, 1784 (1974).